AGU PUBLICATIONS

JGR

Journal of Geophysical Research: Space Physics

RESEARCH ARTICLE
10.1002/2014JA020083

Key Points:
- The wake refills along and perpendicular to B, as observed by ARTEMIS
- One-dimensional theory utilizing ion and electron distributions reproduces ARTEMIS data
- One-dimensional theory fails for high beta, reflected protons, and electron anisotropies

Correspondence to:
J. S. Halekas,
jazzman@ssl.berkeley.edu

Citation:
Halekas, J. S., A. R. Poppe, and J. P. McFadden (2014), The effects of solar wind velocity distributions on the refilling of the lunar wake: ARTEMIS observations and comparisons to one-dimensional theory, *J. Geophys. Res. Space Physics*, *119*, doi:10.1002/2014JA020083.

Received 14 APR 2014
Accepted 19 JUN 2014
Accepted article online 24 JUN 2014

The effects of solar wind velocity distributions on the refilling of the lunar wake: ARTEMIS observations and comparisons to one-dimensional theory

J. S. Halekas[1,2], A. R. Poppe[1,2], and J. P. McFadden[1]

[1]Space Sciences Laboratory, University of California, Berkeley, California, USA, [2]Solar System Exploration Research Virtual Institute, NASA Ames Research Center, Moffett Field, California, USA

Abstract The lunar plasma wake refills from all directions, with processes operating both parallel and perpendicular to the magnetic field. The resulting wake structure depends sensitively on the properties of the flowing plasma, including the form of the ion and electron velocity distributions. In this manuscript, we discuss theoretical approximations for the refilling of the lunar wake along the magnetic field. While an often-used treatment for the parallel refilling assumes cold ions, one can derive solutions for arbitrary ion velocity distributions. Similarly, though the most tractable theory utilizes Maxwellian electrons, one can derive solutions for other types of distributions. We discuss the theoretical framework for various one-dimensional solutions, spanning the full range from cold-ion theories to gas-dynamic solutions, and utilizing both Maxwellian and kappa electron distributions. We compare these solutions to ARTEMIS observations of the lunar wake, for time periods with appropriate plasma parameters. We also present cases that reveal the inherent limitations of one-dimensional approximations, including those related to electron anisotropies and those related to perpendicular processes associated with both fluid flow and ion gyro-motion.

1. Introduction

The lunar wake provides a natural example of the expansion of plasma into a vacuum. As plasma flows past the Moon, it encounters a sharp boundary between the undisturbed plasma and the trailing void established by plasma absorption and/or neutralization at the dayside surface. Because of the pressure gradient across this discontinuity, plasma expands into the vacuum as it flows downstream. Many spacecraft have observed the refilling of the lunar wake, including the Explorer 35 and the Apollo sub-satellites (as reviewed by *Ness* [1972] and *Schubert and Lichtenstein* [1974]), the Wind spacecraft [*Ogilvie et al.*, 1996], and the low-altitude polar orbiting spacecraft Lunar Prospector [*Halekas et al.*, 2005, 2011a, 2011b], Kaguya [*Nishino et al.*, 2009a, 2009b, 2010], and Chandrayaan [*Futaana et al.*, 2010]. Most recently, the two ARTEMIS probes [*Angelopoulos*, 2011] have made over a thousand orbits through the lunar wake at a wide range of downstream distances, providing a new perspective on the lunar wake [*Halekas et al.*, 2011c, 2014; *Zhang et al.*, 2012, 2014].

Modelers have applied numerous simulation techniques to plasma wakes, including Vlasov simulations [*Umeda et al.*, 2011], 1-d and 2-d particle-in-cell (PIC) simulations [*Farrell et al.*, 1998; *Birch and Chapman*, 2002; *Kimura and Nakagawa*, 2008; *Nakagawa and Kimura*, 2011; *Nakagawa*, 2013], and 2-d and 3-d hybrid simulations [*Kallio*, 2005; *Trávnicek et al.*, 2005; *Wang et al.*, 2011; *Wiehle et al.*, 2011; *Holmstrom et al.*, 2012] (see *Halekas et al.* [2014] for a more comprehensive review). Each of these models contains a tremendous amount of physics (so much that one must do "data analysis" to understand the results of the simulation), but each also employs approximations. Each also expends considerable computer resources, and only recently has anyone published time-dependent wake simulations [*Wiehle et al.*, 2011].

Therefore, we find it useful to consider simple theoretical approximations to the wake refilling, since these provide additional physical insight. Also, we can easily and rapidly update them to reflect the constantly changing plasma density and flow direction, magnetic field strength and orientation, etc. encountered by the Moon. Previously, investigators have fruitfully compared 1-d plasma expansion theories appropriate for cold ion distributions to Wind [*Ogilvie et al.*, 1996], Lunar Prospector [*Halekas et al.*, 2005, 2011a], Chandrayaan [*Futaana et al.*, 2010; *Hutchinson*, 2013], and ARTEMIS [*Halekas et al.*, 2011c] observations. In this paper, we consider a variety of 1-d approximations for the plasma expansion along the magnetic field line into the wake, each

appropriate for a different combination of electron and ion velocity distributions, and compare them to observations from ARTEMIS.

2. One-Dimensional Approximations for Plasma Refilling a Vacuum

Gurevich et al. first explored the basic theory for plasma refilling a vacuum, using the approximation of quasi-neutrality [*Gurevich et al.*, 1969; *Gurevich and Pitaevsky*, 1975]. In this work, we follow their conventions in normalizing variables and setting up the equations, by defining the normalized variables:

$$u = v\sqrt{M/2T_e}, \quad \tau = s/t\sqrt{M/2T_e}, \quad \psi = e\varphi/T_e, \quad \beta = \frac{T_e}{T_i}. \tag{1}$$

In these normalized self-similar variables (with M the ion mass, T_i the ion temperature, T_e the electron temperature, e the electron charge, φ the electrostatic potential, v the ion velocity, s the distance from the original plasma-vacuum discontinuity, and t the expansion time), using a normalized ion distribution function g, the ion continuity and momentum equations can be combined to give:

$$(u-\tau)\frac{\partial g}{\partial \tau} - \frac{1}{2}\frac{\partial g}{\partial u}\frac{\partial \psi}{\partial \tau} = 0. \tag{2}$$

We can then write the equation of the characteristics:

$$\frac{du}{d\tau} = \frac{1}{2}\frac{F(\tau)}{u-\tau}. \tag{3}$$

We require an expression for the normalized electric force F to solve this equation. In the case of a Maxwellian electron distribution the following expression, equivalent to the Boltzmann equation, holds (assuming quasi-neutrality):

$$F(\tau) = -\frac{d\psi}{d\tau} = -\frac{1}{n}\frac{dn}{d\tau}. \tag{4}$$

We can solve equations (3) and (4) by integrating along the characteristics, using a normalized Maxwellian ion distribution function (written as $g = \mathrm{e}^{-\beta u^2}$ in our normalized variables) as the boundary condition in the undisturbed plasma outside of the rarefaction region.

For the more general case of a kappa electron distribution, we can proceed analogously, with a slightly different electric force term (we can derive this, and similar force expressions for arbitrary electron distributions, by solving for the partial density as a function of electrostatic potential, and taking the derivative):

$$F(\tau) = -\left(\frac{2\kappa-3}{2\kappa-1}\right)\frac{dn}{d\tau}n^{\left(\frac{1+2\kappa}{1-2\kappa}\right)}. \tag{5}$$

Gurevich and Pitaevsky [1975] found the analytic solution of the expansion equations for the case with Maxwellian electrons and cold ions ($\beta = \infty$):

$$n = e^{-\sqrt{2}\tau-1}, \quad u = \tau + \frac{1}{2} \quad \left(\tau > -\frac{1}{\sqrt{2}}\right). \tag{6}$$

This solution, with an exponential reduction in density and a linearly increasing acceleration of the ions into the void, has been re-derived and utilized by numerous authors [e.g., *Samir et al.*, 1983; *Ogilvie et al.*, 1996]. *Halekas et al.* [2005, 2011a] also derived a similar set of equations for cold ions and kappa electron distributions, which we will not repeat here.

Meanwhile, in the opposite extreme, the zero-electric field, gas-dynamic approximation ($\beta = 0$), we can write the solution as (normalizing τ by the ion temperature rather than the electron temperature, to avoid division by zero):

$$n = 0.5(1 - \mathrm{Erf}(\tau_I)). \tag{7}$$

Gurevich and Pitaevsky [1975] also presented numerical solutions of the general result for Maxwellian ions and electrons, each with a finite temperature. For this paper, we have similarly calculated numerical solutions for this warm ion case and have also computed the full warm ion solutions for kappa function electron

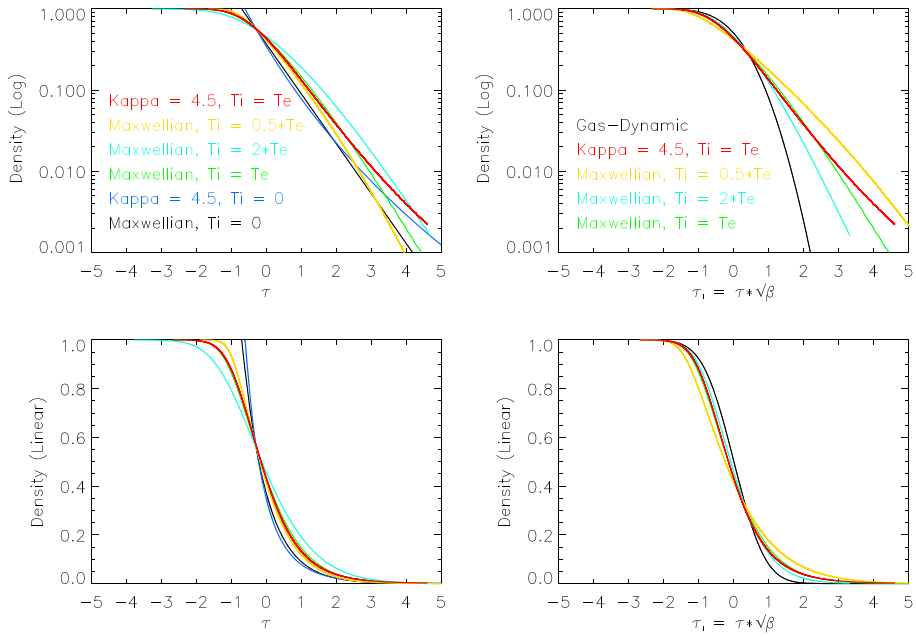

Figure 1. A comparison of seven different 1-d approximations for the density of plasma refilling a vacuum, on a logarithmic scale in the top panels, and a linear scale in the bottom panels. The left panels use $\tau = s/t\ (M/2T_e)^{1/2}$ as the abscissa, and the right panels use $\tau_i = s/t\ (M/2T_i)^{1/2}$, with s the distance from the initial plasma-vacuum boundary and t the expansion time.

distributions (ions remain Maxwellian). Purely analytic solutions have been calculated for the finite temperature Maxwellian ion case, assuming a constant polytropic index of 1 (isothermal expansion) for both ions and electrons [*Nakagawa*, 2013]. The work of *Gurevich and Pitaevsky* [1975] shows that the polytropic index for ions will in fact vary during the expansion and should asymptote to 2. Meanwhile, Maxwellian electrons have a polytropic index of 1, and kappa electrons have a polytropic index of $(2\kappa - 3) / (2\kappa - 1)$.

We show a few of the resulting family of solutions for density as a function of τ in Figure 1. We note that the finite ion temperature solutions asymptote to the cold-ion solutions at large values of τ but have a more rounded density profile near the edge of the wake (due to the spread in ion velocities), slightly more efficient filling of the region near the edge of the wake, and a broader rarefaction outside the cavity. Lower values of β (comparatively warmer ions) result in more significant deviations from the cold-ion solutions. Kappa function electron solutions show only minor differences at the outer edge of the wake but predict significantly higher density in the innermost region of the wake. The gas-dynamic solution, on the other hand, has the greatest density in the outer wake, but the lowest density in the innermost region of the wake.

In Figure 2, we show the ion and electron velocity distributions corresponding to five of the seven solutions shown in Figure 1 (all but the $\beta = 2$ and $\beta = 0.5$ curves). As expected, the velocity distributions for the $\beta = 1$ case lie intermediate between the $\beta = 0$ (gas-dynamic) and $\beta = \infty$ (cold-ion) cases. For the gas-dynamic case, we can interpret the spectra in terms of a simple velocity cutoff. Given the lack of an electric field force or other source of acceleration, only ions with $u > \tau$ can reach a given point in the wake. For the intermediate cases, we still see the effects of this ion velocity filtration but coupled with the acceleration from the electric field. This has the effect of bunching the ions, so that at high values of τ, the distribution asymptotes to the cold-ion solution, as we saw in the density in Figure 1. This parallel cooling of the ion distribution agrees with that predicted by double adiabatic theory [*Clack et al.*, 2004].

We note that while the effective temperature of the electron distribution for the Maxwellian cases remains constant, in the kappa electron case it increases as a function of τ, as a result of electron velocity filtration (this effect is not easily seen without an explicit moment computation). *Halekas et al.* [2005] previously showed that this behavior more closely matched the electron temperature observed in the wake by Lunar Prospector.

All of the approximations presented in Figures 1–2 assume quasi-neutrality. Several studies have discussed the effects of non-neutrality [*Crow et al.*, 1975; *Denavit*, 1979; *Singh and Schunk*, 1982; *Manfredi et al.*, 1993;

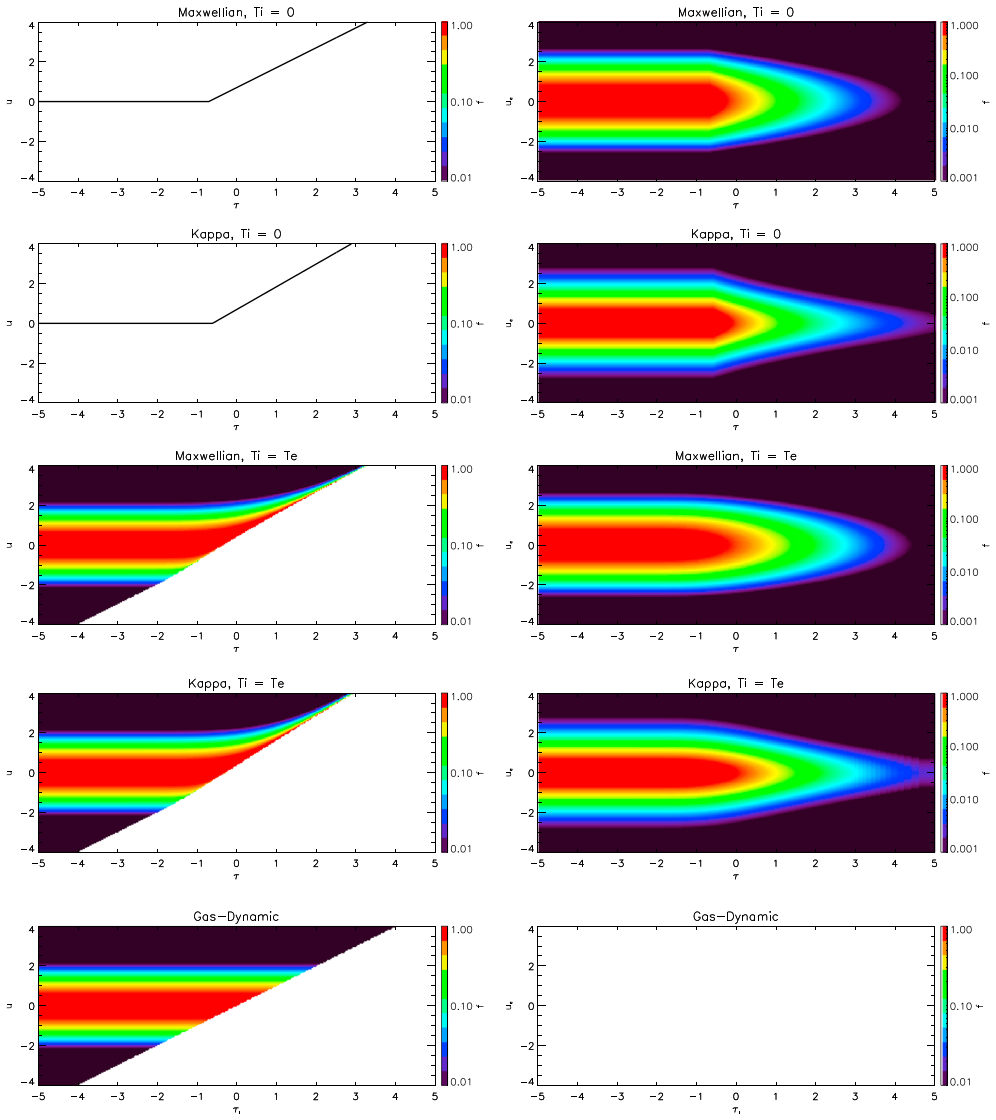

Figure 2. A comparison of velocity distribution functions for five of the theories of Figure 1. The left column shows normalized ion distributions in a logarithmic color scale, and the right shows similarly normalized electron distributions. The top four rows use $\tau = s/t\,(M/2T_e)^{1/2}$ as the *x* axis, and the bottom row uses $\tau_i = s/t\,(M/2T_i)^{1/2}$. Ion velocities use a corresponding normalization, while we express electron velocities in units of the electron thermal velocity $(m_e/2T_e)^{1/2}$.

Sack and Schamel, 1987]. Non-neutrality primarily affects the leading edge of the expansion front (high values of τ), and it remains debatable how much this affects the global structure of the lunar wake, though some work has suggested its importance in the central wake [*Farrell et al.*, 1998; *Nakagawa*, 2013].

We also do not take into account the shape of the Moon, though some observations [*Futaana et al.*, 2010] and theory [*Hutchinson*, 2013] suggest the importance of this factor in some cases. The theory presented here essentially treats the Moon as an occulting disk (a better approximation for higher Mach number flows).

Finally, this theory only describes the free expansion of plasma into the wake along the magnetic field lines. We do not include any effects of gyro-motion, or any perpendicular motion of the plasma or magnetic field lines. As shown in numerous simulations [e.g. *Holmstrom et al.,* 2012; *Wang et al.,* 2011; *Wiehle et al.,* 2011] and confirmed by observations [*Halekas et al.,* 2014], the wake also refills in the direction perpendicular to the magnetic field, in a more fluid fashion, resulting in compression of the field in the central wake. *Zhang et al.* [2014] have shown that the magnitude of this magnetic field compression depends on plasma beta, as expected given basic considerations of pressure balance. In extreme cases, compression factors of over a

factor of 2 can result for very high beta plasmas [*Poppe et al.*, 2014]. Any significant perpendicular compression effects reduce the fidelity of the approximations we use in this work, by changing the magnetic field geometry that the parallel infilling takes place in, and compressing the refilling plasma in the perpendicular direction. We will discuss such a case in section 4.2.

3. Comparing One-Dimensional Approximations to ARTEMIS Observations

3.1. Computing One-Dimensional Approximations

In order to compare the 1-d theories discussed above to ARTEMIS observations, we must calculate the relevant wake coordinates and initial conditions, compute the solutions, and then convert the solutions to the appropriate reference frame. To accomplish these tasks, we utilize plasma moments computed onboard from the ARTEMIS ESA instruments [*McFadden et al.*, 2008], using measurements from the upstream probe to define the initial plasma flow velocity and the electron temperature in the undisturbed medium. At each time, taking the magnetic field vectors measured by the FGM instruments [*Auster et al.*, 2008], we find the two points where a straight line extrapolation of the field line passing through the wake probe intersects a point on a cylindrical surface tangent to the lunar limb and parallel to the flow velocity vector (in other words, the projection of the initial plasma-vacuum discontinuity along the flow). These two points, together with the flow speed, allow us to determine the expansion times t from the initial plasma-vacuum discontinuity at each side of the wake. The distance along the field line from these points, meanwhile, defines the expansion distances s from each side of the wake. Combining these terms, and using the upstream electron temperature, we compute the wake coordinates τ associated with refilling from the two flanks. We evolve these coordinates as a function of time, taking into account the varying flow velocity and magnetic field geometry, and the motion of the ARTEMIS probe, and compute the solutions.

The one-dimensional solutions allow us to determine plasma density, ion flow velocity, and electron temperature, as a function of time. We assume that the refilling populations do not interact in any way (a better approximation for shorter expansion times, and progressively worse farther downstream as the refilling ion beams begin to interpenetrate) and superpose the two solutions associated with refill from the two sides of the wake. We also convert the results (valid in the plasma frame) to the Moon frame, by performing a vector addition with the unperturbed upstream flow velocity. We do not take into account the small (few 10's of km/s) reduction in flow velocity in the wake associated with the pressure gradient parallel to the flow [*Zhang et al.*, 2014].

3.2. Preparing ARTEMIS Data for Comparisons

In order to compare with the solutions derived above, we must make several corrections to the raw measurements. First, we correct vector quantities for spin-phase drift resulting from the loss of the sun pulse in shadow and thermally driven changes in the spacecraft spin, using the methods described by *Georgescu et al.* [2011]. Next, we remove background counts from the ion distributions. Backgrounds due to cosmic rays and natural radioactivity in the ESA microchannel plate detectors do not typically affect plasma moments in the solar wind significantly, but in the wake, where background rates reach levels comparable to or even exceeding real ion counts, careful background subtraction becomes crucial for determining plasma moments (see *Halekas et al.* [2014] for more discussion). After subtracting background, we utilize the quasi-neutral assumption in order to compute the spacecraft potential (by deriving the shift in the distribution required for the electron density moment to agree with the ion density). This potential does not affect the supersonic ions to any great degree but has significant effects on the thermal electron distributions. Once we arrive at an estimate of the spacecraft potential, we can then correct the electron distributions and thus all electron moments using this parameter.

Some discussion on the subtleties of working with ARTEMIS ESA data in the solar wind and wake seems in order. For the ARTEMIS probes, the ESA instruments generally operate in magnetospheric mode [*McFadden et al.*, 2008], which has 32 energy sweeps per spin, each with 32 energy bins logarithmically spaced from ~5 eV to ~25 keV. The data processing unit uses the 32×32 distribution to compute moments onboard and then re-bins it into smaller arrays to reduce data volume before transmission. In the spin plane, given the 11.25 degree spacing of the energy sweeps, and the ~6 degree full width at half maximum (FWHM) intrinsic resolution, the measurements unevenly sample the distribution as a function of the spin-plane angle. Therefore, for very cold ion populations, some overestimation or

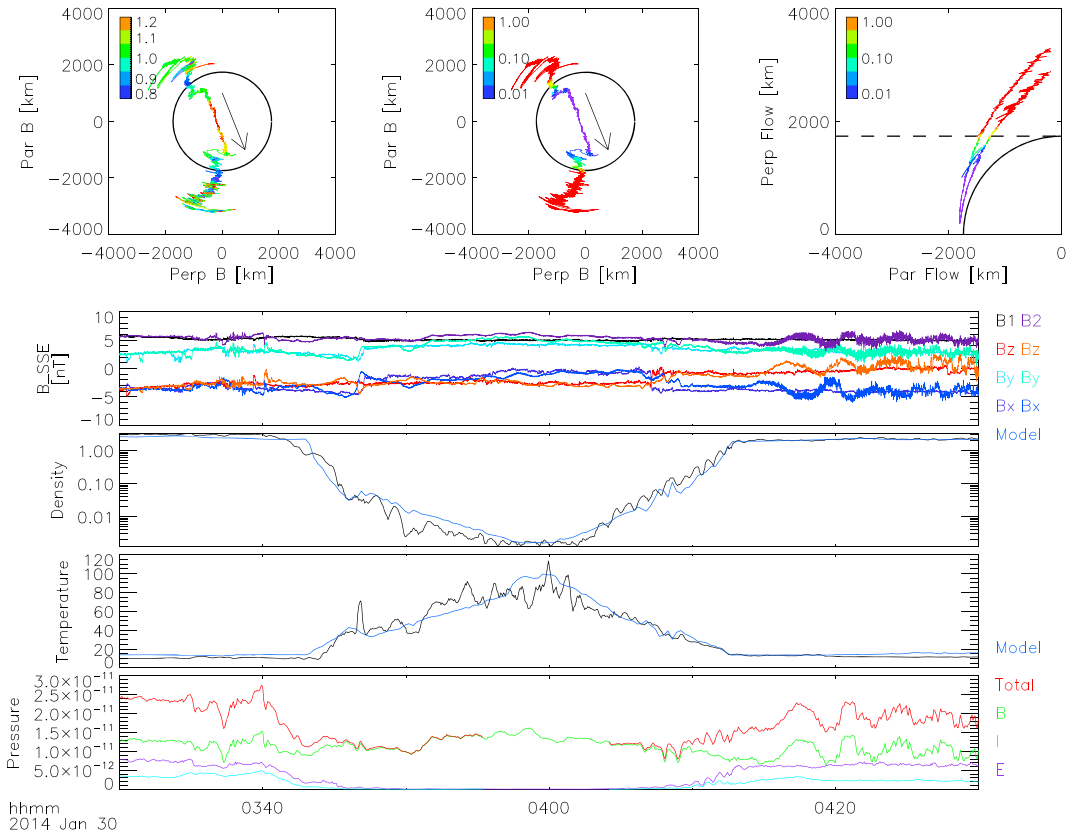

Figure 3. The top three panels show the ARTEMIS P2 trajectory in a wake coordinate system (with the flow antiparallel to the *x* axis and the magnetic field in the *x-z* plane), showing magnetic field magnitude and ion density (cm^{-3}) normalized to upstream values for a cross section of the wake and density in cylindrical coordinates. The time series panels show the magnetic field magnitude and components for upstream and downstream probes (B1 refers to the magnetic field from P1, and B2 the field from P2, etc.), ion density and electron temperature (eV) measured by the downstream probe P2, compared to a 1-d cold-ion approximation for electrons with a kappa distribution ($\kappa = 4.5$), and the perpendicular pressure (Pa) components measured by the wake probe associated with the magnetic field, the ion and electron thermal motion, and the total. We determine the ion temperature using a two-component fit to the convecting protons and alpha particles.

underestimation (depending on the velocity angle relative to clocking of the spin-plane angle bins) of the ion density can occur. For typical solar wind temperatures and normally low levels of variability in the velocity angle in the undisturbed solar wind, we can generally use the ARTEMIS measurements with few corrections. However, in the wake, the spin-plane bins drift with time (as a result of the loss of the sun pulse), which can produce spurious oscillations as the measurement successively under- and oversamples the peak of the distribution. Parallel cooling of the ion distribution during the wake refilling process exacerbates this issue. These issues can affect the ion velocity and density computations. Since we use ion density to find the spacecraft potential and correct electron distributions, this can also propagate to those values.

Though not a figure of merit for most comparisons, the ion temperature proves a useful quantity for diagnostic purposes. Unfortunately, given the limited energy and angle resolution of the instruments in magnetospheric mode, ESA measurements usually cannot fully resolve cold ion distributions, particularly in a high Mach number flow. Therefore, in the solar wind, we generally must use a fitting routine to estimate the true ion temperature. To accomplish this, we fit to a convolution of the ESA intrinsic resolution with a sum of two convecting Maxwellian distributions, representing the protons and alpha particles, in order to estimate both alpha abundance and proton temperature. In the magnetosheath, given higher ion temperatures (lower Mach numbers), we need not employ this fitting procedure.

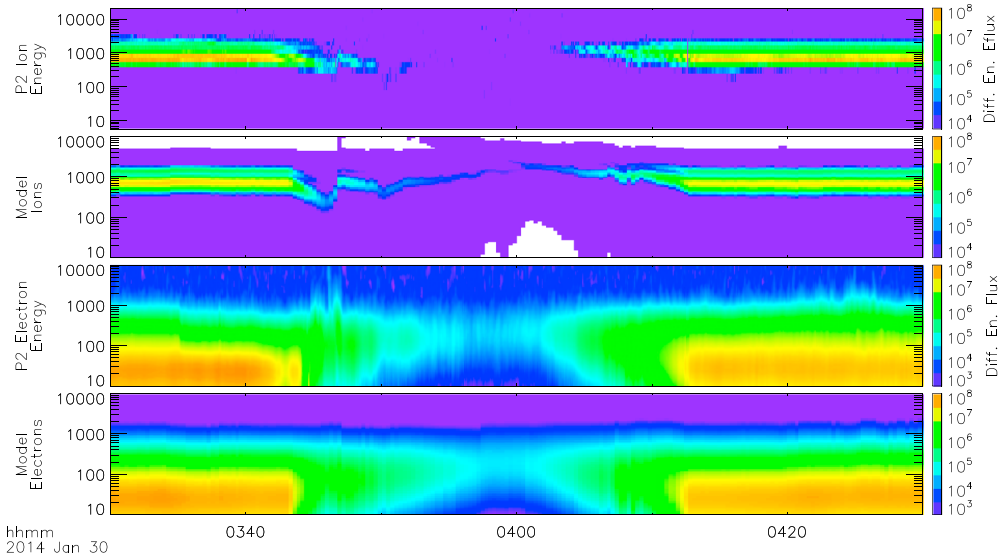

Figure 4. Ion and electron energy spectra measured by ARTEMIS P2 during the time period shown in Figure 3, in units of differential energy flux [eV/(cm^2 s sr eV)], compared to theoretical predictions using the same approximation as Figure 3.

3.3. Comparisons to Cold-Ion Refilling Theory

For the conditions most commonly encountered by ARTEMIS in the solar wind, the cold-ion ($\beta = \infty$) refilling approximations described in section 2 often match the observations rather well. Figure 3 shows an example comparison. For this case, the electron pressure exceeds the ion pressure, and the perpendicular pressure associated with the magnetic field exceeds both ion and electron pressure (total plasma beta on the order of unity). As a result, parallel processes dominate the wake refilling, ion thermal velocity effects prove relatively unimportant, and cold-ion theory does a good job of matching observations. The trajectory of the ARTEMIS probe through the central wake close to the plane of the magnetic field also helps to minimize the effect of any perpendicular compression.

Given these favorable conditions, the plasma density and electron temperature calculated from the cold-ion theory described in section 2 match the observations extremely well (taking into account a finite ion temperature does not improve the agreement). The increase in electron temperature in the wake requires the use of kappa electron distributions to reproduce (Maxwellian electron distributions would result in a constant temperature in the wake). We note a low level of spurious oscillations in the measured plasma density, resulting from the spin-phase drift effects and angular under-sampling described in section 3.2, on the exit side of the wake. The large-scale magnetic field oscillations seen outside the wake on the exit side may result from the presence of crustal magnetic fields upstream and/or ions reflected from those crustal fields; however, these interesting effects lie beyond the scope of this paper and do not in this case appear to affect the refilling of the wake.

In addition to plasma moments, we can compare ion and electron energy spectra, as shown in Figure 4. For this comparison, we employ several approximations. For ions, we take a constant ion temperature of 10 eV (strictly speaking, the theory used for this comparison assumes zero ion temperature, but the real ion distribution has a temperature on this order). We also add a second component to the ion distribution, corresponding to a 3% abundance of alpha particles, in accord with the results of a two-component fit to the ion distribution (as described in section 3.2). For electrons, we correct the measured spectra for spacecraft potential (also described in section 3.2) and compute model spectra assuming pure kappa function distributions. We find a rather good match for both electron and ion spectra, including good agreement with observed changes in the ion velocity associated with variations in the magnetic field as the probe traverses the wake. The one-dimensional solutions slightly overestimate the abundance of refilling plasma in the central wake, possibly because we have not taken into account any interaction of the two refilling populations, which would tend to reduce the electric field and slow the refilling. We also note that the ESA observations in the central wake have very low counting statistics, making it difficult to observationally resolve such a tenuous ion beam.

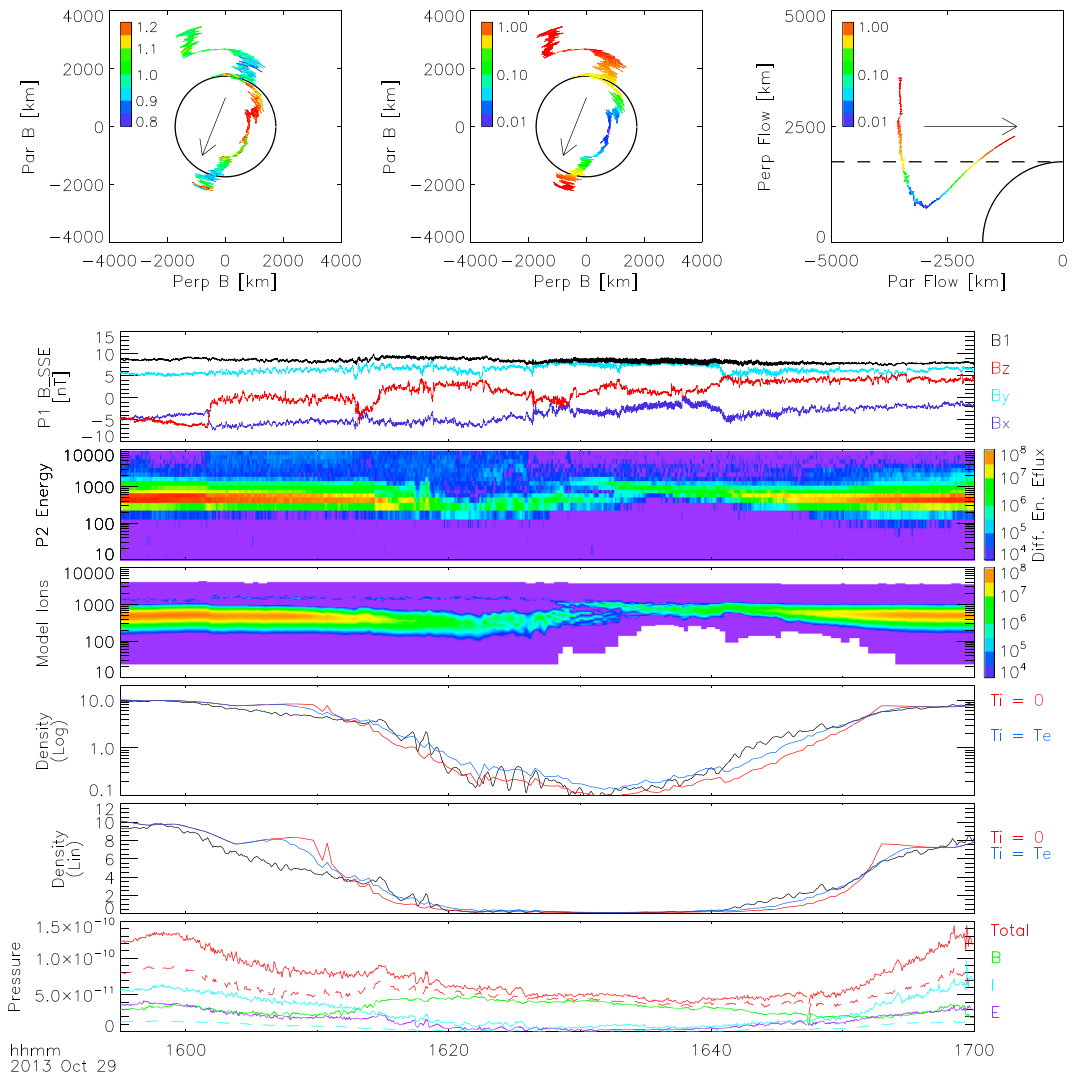

Figure 5. The top panels show the ARTEMIS P2 trajectory in the same format as Figure 3. The time series panels show the magnetic field for the upstream probe P1, ion spectra measured by P2, modeled ion spectra for $T_i = T_e$ and $\kappa = 4.5$, measured ion density compared to models with $T_i = 0$ and $T_i = T_e$, on logarithmic and linear scales, and the perpendicular pressure in the same format as Figure 3. In the bottom panel, solid lines show results using ion temperatures from a direct integration, and dashed lines show results using a two-component fit as in Figure 3.

3.4. Comparisons to Warm-Ion Refilling Theory

During time periods with more significant ion temperatures, we need to utilize the full warm-ion theory described in section 2. To compare to observations, we compute a numerical solution for a finite value of the temperature ratio β. In addition to a better approximation for the density, this allows us to compute ion energy spectra with a more realistic temperature, allowing a more sophisticated comparison. For these comparisons, we have not included an alpha component, though in principle this could also lead to a slightly better match in the spectra.

We show a comparison of a case where $T_i \sim T_e$, in Figure 5. For this time period, we cannot determine the ion temperature with great accuracy. If we calculate moments by integration, we find that $T_i \sim 2T_e$; however, as we have discussed, moment computations overestimate ion temperature in the solar wind (due to the limited instrumental resolution). If we instead rely on the fitting procedure described in section 3.2, we find that $T_i \sim T_e/2$. However, this fit neglects any significant flux outside the core. During this wake crossing, the Moon traversed the Earth's foreshock, resulting in a significant population of reflected ions at energies above

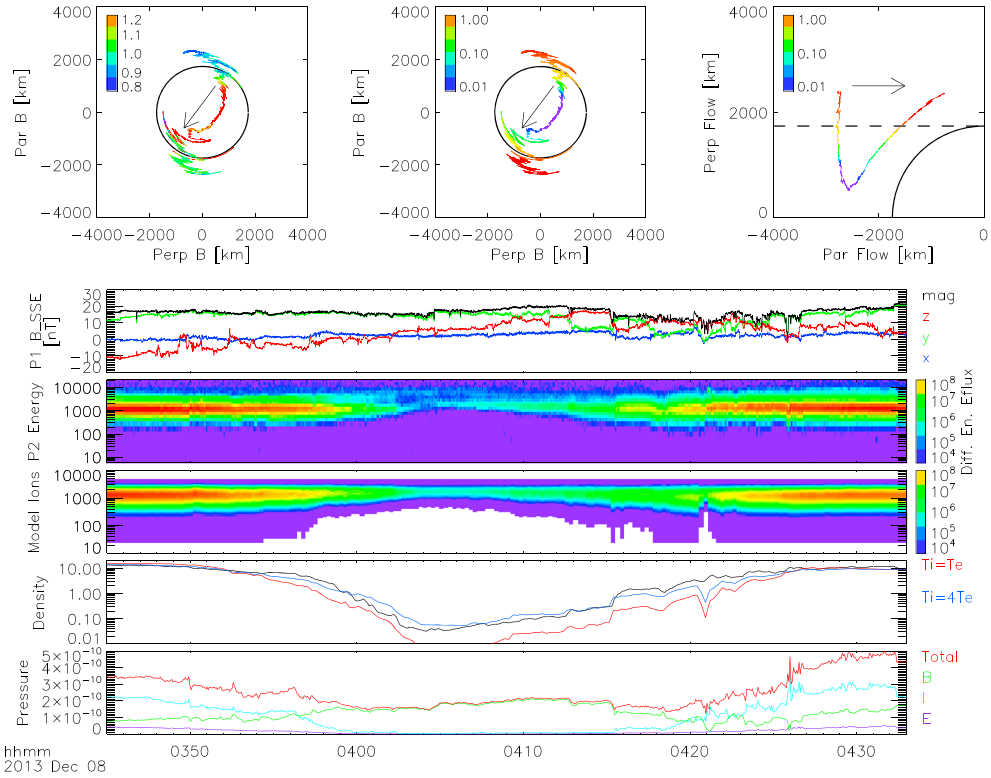

Figure 6. The top panels show the ARTEMIS P2 trajectory in the same format as Figure 3. The time series panels show the magnetic field for the upstream probe P1, ion spectra measured by P2, modeled ion spectra for a 1-d approximation with Maxwellian electrons with $T_i = 4T_e$, measured ion density compared to models for $T_i = T_e$ and $T_i = 4T_e$, and perpendicular pressure in the same format as Figure 3. The ion temperature used in the bottom panel is determined from a direct integration.

the main core population. Therefore, the true bulk ion temperature should lie somewhere between the results of the moment computation and the fit to the core. As a compromise, we assume $T_i \sim T_e$ when computing the one-dimensional solution. We show the resulting model ion spectra along with the observed spectra, along with a density comparison to both the full warm-ion theory and the cold-ion approximation, in Figure 5. We note that, in the central wake, both approximations match the observations fairly well, since the warm-ion case rapidly asymptotes to the cold-ion result. However, the warm-ion theory does a much better job of matching the density at the edge of the wake, where the dispersion in ion velocities has the greatest effect. Intriguingly, at the wake entry, even the warm-ion theory does not match the form of the density rarefaction. This may result from the significant energetic ion population observed at that time, which could cause a higher effective rarefaction speed; however, it could also account from other factors not accounted for by the one-dimensional approximations, such as finite gyro-radius effects.

At some rare times, the ion temperature greatly exceeds the electron temperature. The Moon sometimes encounters this condition in the Earth's magnetosheath. We show an example in Figure 6, for a time with $T_i \sim 4T_e$ (a very high temperature ratio, unusual even in the sheath). We find that the warm ion theory again does a good job of matching the observed spectra and density, with the best match for the actual temperature ratio, providing confidence in the approximations used. We note that a high plasma beta naturally accompanies the high ion temperature. In principle this implies that perpendicular compression of the field should prove significant. Indeed, we observe a rather large increase in the magnetic field in the wake (see the upper left panel of Figure 6, and magnetic field pressure component in the bottom panel). However, this does not perturb the results significantly in this case, since the probe orbit lies in the plane of the field, and so the perpendicular compression does not significantly change the geometry of the field encountered by the probe. The increase in magnetic field should also lead to some mirroring of the electrons, but this does not appear to affect the refilling enough to greatly degrade the comparison. In section 4.2, we will show an orbit for a similar set of

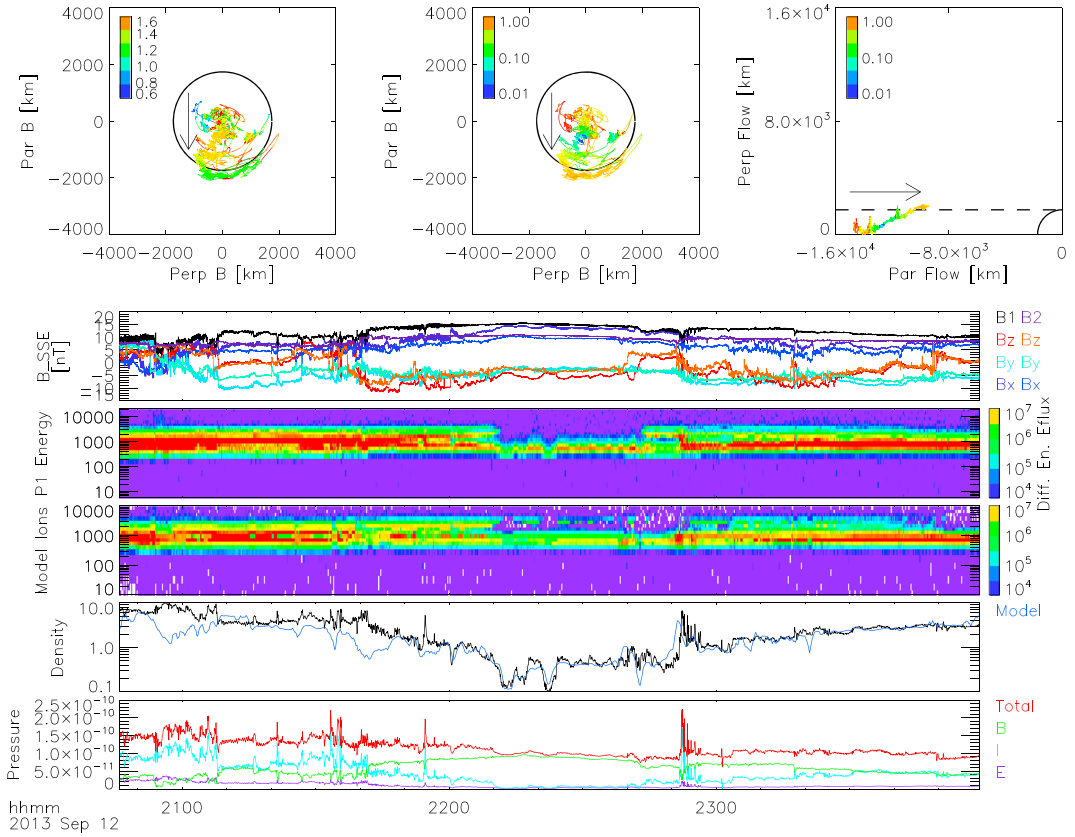

Figure 7. The top panels show the ARTEMIS P1 trajectory in the same format as Figure 3. The time series panels show the magnetic field for the upstream and downstream probes, the ion spectra measured by P1, modeled ion spectra for a 1-d gas-dynamic calculation, measured ion density compared to the gas-dynamic model, and perpendicular pressure in the same format as Figure 3. The ion temperature used in the bottom panel is determined from a direct integration.

parameters but in the plane perpendicular to the magnetic field. In that case, we will find much greater discrepancies between observation and one-dimensional theory, as one would expect.

3.5. Comparisons to Gas-Dynamic Refilling Theory

At greater distances down the wake, the refilling ion populations from the two flanks completely interpenetrate. Electric field effects should thus become significantly less important at these distances, particularly during times with high ion temperatures, which already minimize the effects of electric fields. For such cases, we can at times use a pure gas-dynamic theory with some success. At these times, we can simply take the ion distribution measured upstream and cut it in velocity space according to the travel time condition $u < \tau$, for both parallel and antiparallel ion velocities (corresponding to refilling from the two flanks). We show a comparison of this approximation to ARTEMIS observations in Figure 7, for an orbit well down the wake, at a time with a significant ion temperature (~50 eV). The spectra and density computed from the travel time condition match the measured values for much of the wake crossing, even at times with significant variability in the upstream conditions. The gas-dynamic model reproduces the two-component form of the spectra in the wake, which results from the interpenetration of the refilling populations from the two flanks. Before ~22:00, we observe larger densities than expected from simple one-dimensional approximations, particularly given the inferred position in the central wake. These enhanced densities could result from ion-ion instabilities driven by the two refilling populations [*Farrell et al.*, 1998]. However, at these large downstream distances, small offsets in velocities and magnetic fields significantly change the predicted location of the wake, resulting in great sensitivity to small measurement errors, and raising the possibility that the unexpected behavior simply results from an inaccurate estimate of the wake orientation.

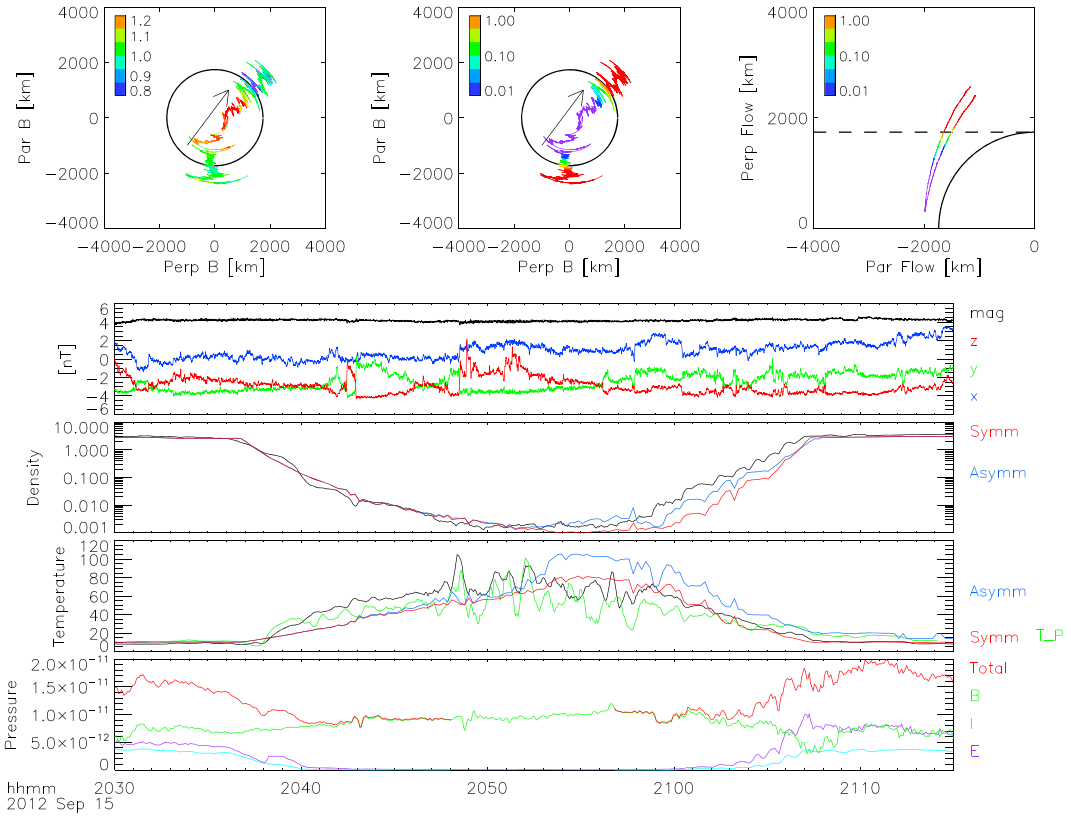

Figure 8. The top panels show the ARTEMIS P2 trajectory in the same format as Figure 3. The time series panels show the magnetic field for the upstream probe P1, ion density, and electron temperature measured by the downstream probe P2 (calculated for the entire electron distribution in black and for pitch angles within 30° of parallel/antiparallel in green), compared to a 1-d cold-ion approximation for electrons with a kappa distribution ($\kappa = 4.5$), for a model assuming isotropic electrons ("Symm") and the same approximation for an electron distribution with a temperature twice as high on the outbound side ("Asymm"), and the perpendicular pressure in the same format as Figure 3. The ion temperature is determined from a two-component fit to the convecting protons and alpha particles.

4. Limitations of One-Dimensional Approximations for Wake Refilling

4.1. The Effects of Suprathermal Electron Anisotropies

The one-dimensional approximations discussed above neglect several important pieces of physics. First, these approximations assume isotropic single-component electron distributions. In contrast, solar wind electron distributions typically have multiple components and significant anisotropy, associated with the core, halo, super-halo, and strahl populations. Accounting for multiple components to the spectra proves relatively easy, merely involving a change to the electric field term in the equations (in essence, re-computing the equivalent of the Boltzmann relation for the given electron distribution). Factoring in electron anisotropy proves more challenging, given the one-dimensional nature of the approximations we have utilized. However, at some times, we can improve the match to observations by simply using two different solutions for the refilling along the directions parallel and antiparallel to the magnetic field. Figure 8 shows an example of such a case. For this wake crossing, the cold-ion theory matches the observations quite well on the entry side of the wake but significantly underestimates the density on the exit side of the wake. In an attempt to correct this mismatch, we calculate the solution for an electron temperature twice the bulk temperature on the exit side, resulting in a much better match to the observed density. This asymmetric approximation does not match the observed bulk temperature but better matches the temperature calculated from the portion of the distribution within 30° of parallel/antiparallel to the magnetic field (except in the central wake, where we still find a discrepancy). As shown in Figure 9, the asymmetric approximation also does a significantly better (though not perfect) job of matching the observed electron and ion energy spectra, particularly the greater flux of infilling ions and the increased electron temperature from 20:53 to 21:12.

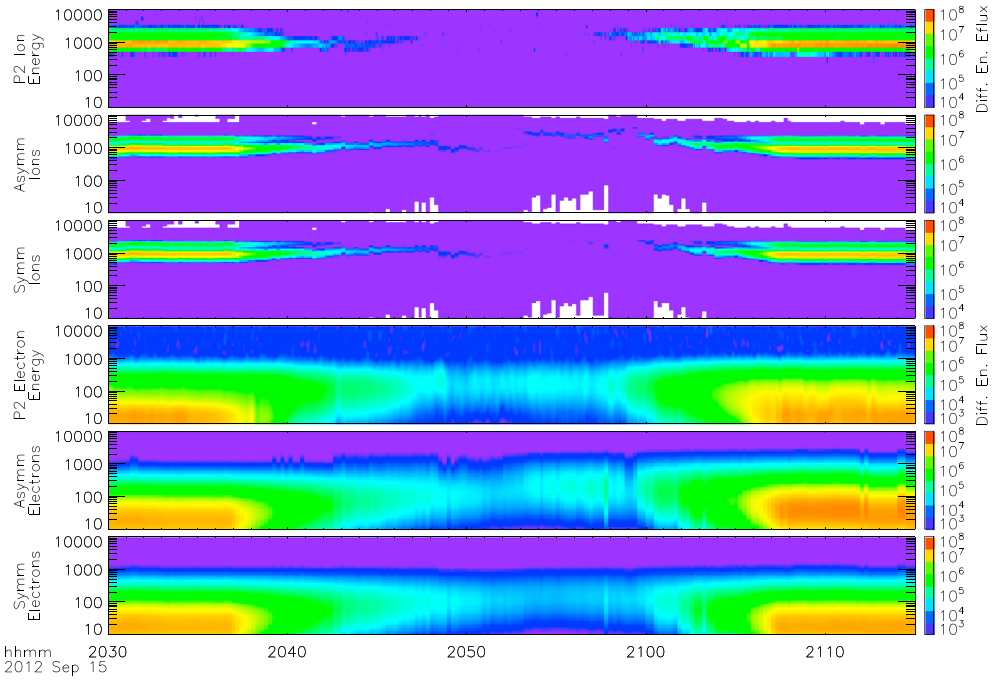

Figure 9. Measured ion and electron energy spectra from ARTEMIS P2 from the time period shown in Figure 8, in units of differential energy flux [eV/(cm^2 s sr eV)], as compared to theoretical predictions using the same two approximations as Figure 8.

In Figure 10, we show measured omnidirectional electron energy spectra at the entry and exit sides of the wake, as well as those corresponding to the portion of the distribution within 30° of parallel/antiparallel to the magnetic field, along with the two sets of model input spectra. We see that the symmetric one-component model does not perfectly reproduce the observed spectrum (which has two components) on either side of the wake but matches in an average sense on the entry side. On the exit side, though, the symmetric model significantly underestimates the temperature of the distribution, particularly the field-aligned portion. As the reader will recognize, this significant anisotropy in the observed electrons results from the strahl component of the distribution. Our result implies that the strahl apparently has a significant effect on the refilling of the wake. By increasing the electron temperature used in our one-dimensional approximation to correspond to that associated with the strahl, we find a better match to the observations, even though the new input spectrum does not match the observed spectrum at low energies.

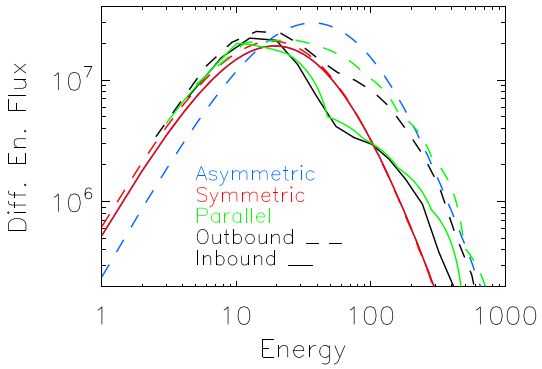

Figure 10. Measured electron distributions (averaged over all pitch angles in black and for pitch angles within 30° of parallel/antiparallel in green) on the inbound and outbound sides of the wake for the wake crossing shown in Figures 8–9, as compared to an isotropic distribution with $\kappa = 4.5$ in red (the input spectrum used for the "Symm" case in Figures 8–9), and a distribution with twice the temperature on the outbound side (the input spectrum used for the "Asymm" case in Figures 8–9).

As we can see in the pressure components in the bottom panel of Figure 8, this wake crossing displays some magnetic field compression, associated with perpendicular refilling of the wake. This has at least two effects worth noting. First, the increase in the field will mirror electrons with low parallel velocities, ensuring that the more nearly field-aligned component forms a greater portion of the distribution in the central wake and helping explain why the strahl has a seemingly incommensurate effect on the refilling.

In addition, perpendicular compression may explain the slight discrepancy remaining between the one-dimensional approximation

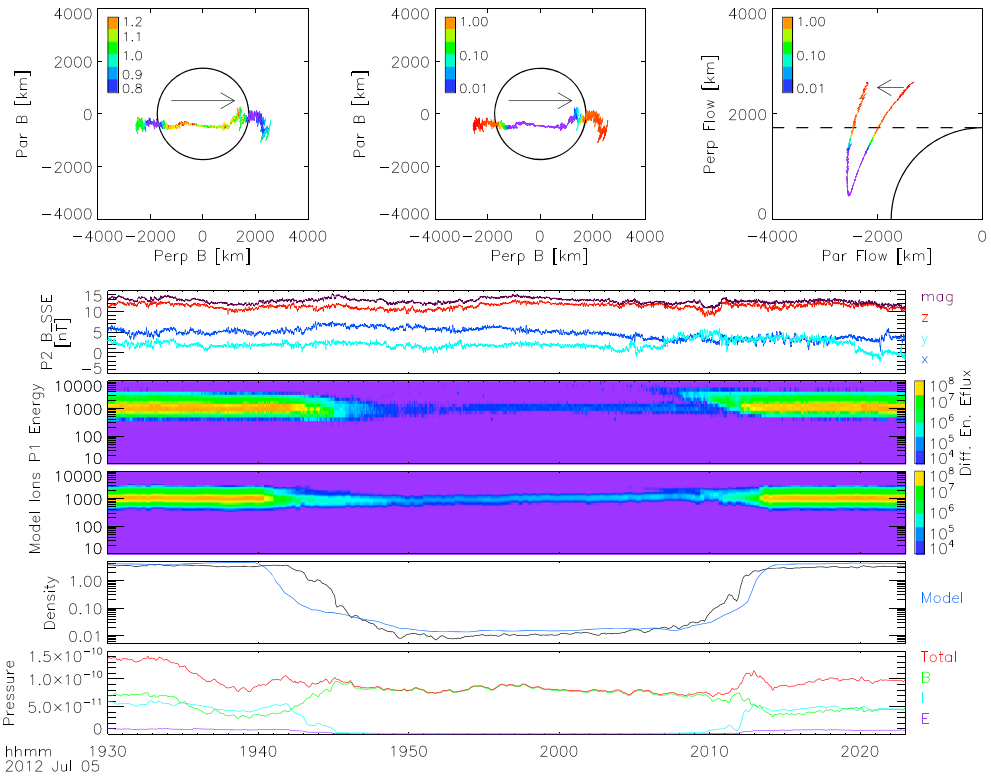

Figure 11. The top panels show the ARTEMIS P1 trajectory in the same format as Figure 3. The time series panels show the magnetic field for the upstream probe P2, ion spectra measured by P1, modeled ion spectra for a 1-d cold-ion approximation for electrons with a kappa distribution ($\kappa = 4.5$), measured ion density compared to the cold-ion model, and perpendicular pressure in the same format as Figure 3. The ion temperature used in the bottom panel is determined from a direct integration.

and observations at the exit of the wake. With the increase in the effective electron temperature, the one-dimensional solution matches the observed slope in density, but a small lateral offset in position still remains. This offset likely results from perpendicular compression and shows up only at the exit side because the magnetic field geometry ensures that the probe trajectory takes it through the perpendicular flank of the wake (whereas the input trajectory lies in the plane parallel to the field). In the next section, we show a much more significant example of this effect.

4.2. The Effects of Perpendicular Compression

At times with significant ratios of plasma pressure to magnetic field pressure (plasma beta), refilling of the wake in the direction perpendicular to the magnetic field may prove as or more important than the refilling along the field lines described above. We have already investigated several cases with relatively high plasma beta in sections 3 and 4.1; however, in most of those cases the probe orbit lay close to the plane of the magnetic field, minimizing the effects of perpendicular compression on the wake refilling. In Figure 11 we show a case where the probe orbit lies in the plane perpendicular to the magnetic field, at a time with significant plasma beta. In this case, we find that the one-dimensional parallel refilling approximation, though it captures the form of the density and ion spectra in a general sense, significantly overestimates the width of the wake at the downstream distance sampled by the ARTEMIS probe. The narrower observed width most likely stems from the inward motion of flux tubes in response to the pressure gradient perpendicular to the magnetic field, which results in compression of the magnetic field in the central wake. We can easily understand this phenomenon in a fluid or MHD picture, even in a one-dimensional approximation (with the dimension perpendicular to the field rather than parallel as in the theories described previously). In the full three-dimensional lunar wake, of course, we must consider refilling both parallel and perpendicular to the magnetic field, with the latter more important for cases with high plasma beta. We also observe a recompression in the plasma pressure observed near the edge of the cavity. This most likely results from the

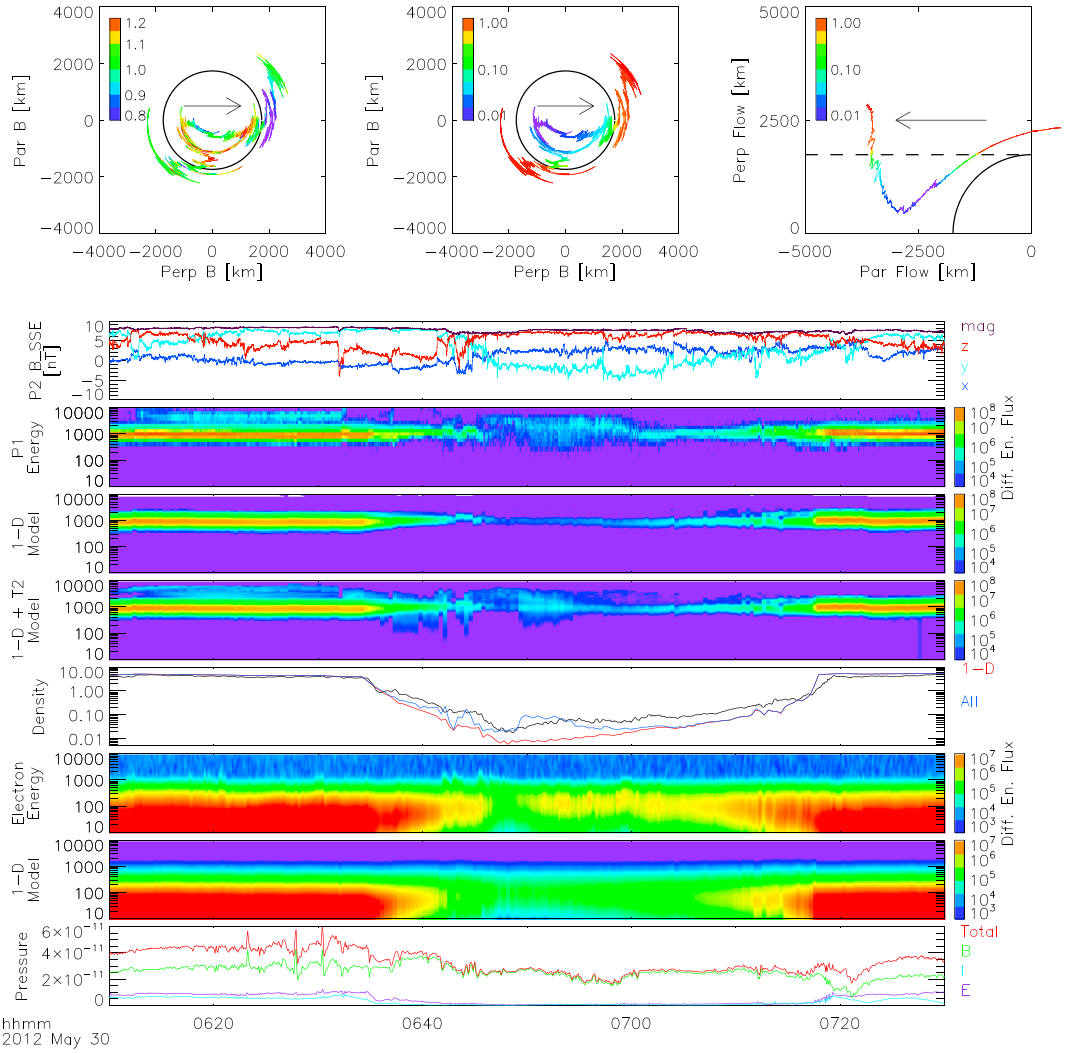

Figure 12. The top panels show the ARTEMIS P1 trajectory in the same format as Figure 3. The time series panels show the magnetic field for the upstream probe P2, ion spectra measured by P1, modeled ion spectra for a 1-d cold-ion approximation for electrons with a kappa distribution ($\kappa = 4.5$), spectra from the same model with the addition of a test-particle simulation of solar wind protons reflected from crustal magnetic fields on the dayside, the density measured by P1 as compared to the results of the 1-d cold-ion approximation without ("1-D") and with ("All") a reflected proton component, electron spectra measured by P1, model electron spectra from the 1-d cold-ion model, and perpendicular pressure in the same format as Figure 3. The ion temperature used in the bottom panel is determined from a two-component fit to the convecting protons and alpha particles.

piling up of the refilling plasma against the obstacle formed by the compressed magnetic field in the central void, as predicted from simulations [*Holmstrom et al.*, 2012], and associated with the fast mode wave fronts (current systems) that bound the wake [*Fatemi et al.*, 2013]

4.3. The Effects of Type-II Ion Entry

Another phenomenon that reduces the effectiveness of one-dimensional approximations for wake refilling, like that discussed above in section 4.2, involves plasma motion perpendicular to the plane of the magnetic field. However, unlike the perpendicular motion of flux tubes discussed above, easily understood in a fluid or MHD framework, this involves fundamentally kinetic processes. As described effectively from the observational standpoint by *Nishino et al.* [2009b, 2010] and from the simulation standpoint by *Holmstrom et al.* [2010], solar wind protons that reflect from the dayside lunar surface [*Saito et al.*, 2008] and from crustal magnetic fields [*Saito et al.*, 2010; *Lue et al.*, 2011] feel the effects of the solar wind magnetic field and

convection electric field, and for the right combination of magnetic field geometry and flow velocity, can gyrate into the near lunar wake. We show an ARTEMIS observation of such a case in Figure 12. We see a significant ion population, covering a broad range of energies above and below the main solar wind peak, both inside and outside the lunar wake. Not surprisingly, a one-dimensional solution significantly underestimates the density in the wake. As an instructive exercise, we attempt to account for the effects of the reflected protons by using a test-particle model, while freely acknowledging the inherent non-self-consistency of this approach. We launch reflected protons from above the dayside lunar surface with a weight roughly corresponding to the reflection percentage observed by Kaguya and Chandrayaan (including the effects of reflection from the surface and from crustal magnetic fields), assuming an isotropic reflection function everywhere, and follow these particles in the magnetic field and electric field measured and inferred from ARTEMIS observations, as a function of time, in order to construct ion distributions at the ARTEMIS position. We then add the simulated reflected proton distribution to that calculated from the one-dimensional parallel refilling theory, producing a result that at least qualitatively matches the observed density and ion spectra. However, we do note several discrepancies. The distribution of reflected protons in the wake appears broader than that predicted by our simple model. Furthermore, the density in the central wake and on the exit side exceeds that predicted by the one-dimensional plus test particle model. This most likely results from the perturbation of the wake structure by the reflected protons. As the reflected protons gyrate into the wake, they create a local charge imbalance that electrons must attempt to compensate, by traveling along the magnetic field lines. As a result, the electric field on the field lines populated by the reflected protons changes significantly from that predicted by the one-dimensional approximation and in fact must reverse sign at least locally. While in the typical refilling case electric fields point inward and accelerate ions into the wake, in these regions the electric fields must point outward and accelerate electrons into the wake. We can see the effects of this reversed electric field in the electron spectra (especially from 06:50 to 07:10), which contain a significant population of accelerated electrons completely un-accounted for by the parallel refilling theory. Since this electric field reversal can only exist on field lines passing through the localized regions of the wake where reflected protons penetrate, the overall structure of the wake apparently remains relatively similar despite this local disruption.

5. Conclusions and Implications

In principle, only a full three-dimensional kinetic simulation of the lunar wake can fully reproduce its full structure and complexity. However, for certain cases, we have shown that one can employ one-dimensional approximations for wake refilling to successfully reproduce many features of the observed structure of the lunar wake. One-dimensional approximations do the best job of reproducing the observed wake structure at times with low plasma beta, and/or for orbits that traverse the wake near the plane of the magnetic field. For times with higher plasma beta, particularly for orbits out of the plane of the field, perpendicular infill and magnetic compression significantly perturb the wake structure. Other factors that compromise the fidelity of one-dimensional approximations include electron anisotropies and reflected protons (Type-II entry). Nonetheless, if used appropriately, one-dimensional theories provide a powerful tool for understanding and predicting the structure of plasma wakes. We note that the wakes of the icy moons of Saturn would provide a revealing test case for these theories. Rhea and Tethys have clear plasma wakes, with many similarities to the Earth's Moon [*Khurana et al.*, 2007; *Roussos et al.*, 2007; *Simon et al.*, 2009]. However, in this regime, one would need to utilize theory appropriate for a subsonic flow, for a high ion mass, and for rather significant ratio of ion temperature to electron temperature. One could quite simply modify the parallel theories presented herein for this regime, and they should work rather well given the low plasma beta typically encountered at their orbits. We leave the details for future work, but note that one would most likely need to employ a full numerical solution to take into account the significant ion temperature, rather than using the cold-ion theory often discussed in the literature.

Acknowledgments

We thank NASA's Solar System Exploration Research Virtual Institute (number SSERVI-2014-096) and the LADEE Guest Investigator program through NASA Grant NNX13A071G for support and also thank ISSI for hosting a workshop that inspired part of this work. We acknowledge NASA contract NAS5-02099 and V. Angelopoulos for use of data from ARTEMIS, and specifically K. H. Glassmeier, U. Auster, and W. Baumjohann for the use of FGM data. ARTEMIS data are publicly available at http://artemis.ssl.berkeley.edu and NASA's CDAWeb.

Yuming Wang thanks Tomoko Nakagawa and an anonymous reviewer for their assistance in evaluating this paper.

References

Angelopoulos, V. (2011), The ARTEMIS mission, *Space Sci. Rev.*, *165*, 3–25, doi:10.1007/s11214-010-9687-2.

Auster, H. U., et al. (2008), The THEMIS fluxgate magnetometer, *Space Sci. Rev.*, *141*, 235–264.

Birch, P. C., and S. C. Chapman (2002), Two dimensional particle-in-cell simulations of the lunar wake, *Phys. Plasmas*, *9*, 1785–1789.

Clack, D., J. C. Kasper, A. J. Lazarus, J. T. Steinberg, and W. M. Farrell (2004), Wind observations of extreme ion temperature anisotropies in the lunar wake, *Geophys. Res. Lett.*, *31*, L06812, doi:10.1029/2003GL018298.

Crow, J. E., P. L. Auer, and J. E. Allen (1975), The expansion of plasma into a vacuum, *J. Plasma Phys.*, *14*, 65–76.

Denavit, J. (1979), Collisionless plasma expansion into a vacuum, *Phys. Fluids*, *22*, 1384.

Farrell, W. M., M. L. Kaiser, J. T. Steinberg, and S. D. Bale (1998), A simple simulation of a plasma void: Applications to Wind observations of the lunar wake, *J. Geophys. Res.*, *103*, 23,653–23,660, doi:10.1029/97JA03717.
Fatemi, S., M. Holmstrom, Y. Futaana, S. Barabash, and C. Lue (2013), The lunar wake current systems, *Geophys. Res. Lett.*, *40*, 17–21, doi:10.1029/2012GL054635.
Futaana, Y., S. Barabash, M. Wieser, M. Holmström, A. Bhardwaj, M. B. Dhanya, R. Sridharan, P. Wurz, A. Schaufelberger, and K. Asamura (2010), Protons in the near lunar wake observed by the Sub-keV Atom Reflection Analyzer on board Chandrayaan-1, *J. Geophys. Res.*, *115*, A10248, doi:10.1029/2010JA015264.
Georgescu, E., F. Plaschke, U. Auster, K.-H. Fornacon, and H. U. Frey (2011), Modelling of spacecraft spin period during eclipse, *Ann. Geophys.*, *29*, 875–882.
Gurevich, A. V., and L. P. Pitaevsky (1975), Non-linear dynamics of a rarefied ionized gas, *Prog. Aerosp. Sci.*, *16*, 227–272.
Gurevich, A. V., L. P. Pitaevskii, and V. V. Smirnova (1969), Ionospheric aerodynamics, *Space Sci. Rev.*, *9*, 805–871.
Halekas, J. S., S. D. Bale, D. L. Mitchell, and R. P. Lin (2005), Electrons and magnetic fields in the lunar plasma wake, *J. Geophys. Res.*, *110*, A07222, doi:10.1029/2004JA010991.
Halekas, J. S., S. D. Bale, D. L. Mitchell, and R. P. Lin (2011a), Correction to "Electrons and magnetic fields in the lunar plasma wake", *J. Geophys. Res.*, *116*, A07228, doi:10.1029/2011JA016929.
Halekas, J. S., Y. Saito, G. T. Delory, and W. M. Farrell (2011b), New views of the lunar plasma environment, *Planet. Space Sci.*, *59*, 1681–1694, doi:10.1016/j.pss.2010.08.011.
Halekas, J. S., et al. (2011c), First results from ARTEMIS, a new two-spacecraft lunar mission: Counter-streaming plasma populations in the lunar wake, *Space Sci. Rev.*, *165*, 93–107, doi:10.1007/s11214-010-9738-8.
Halekas, J. S., D. A. Brain, and M. Holmstrom (2014), The Moon's plasma wake, in *Magnetotails in the Solar System*, edited by A. Keiling, AGU, Washington, D. C., in press.
Holmstrom, M., M. Weiser, S. Barabash, Y. Futaana, and A. Bhardwaj (2010), Dynamics of solar wind protons reflected by the Moon, *J. Geophys. Res.*, *115*, A06206, doi:10.1029/2009JA014843.
Holmstrom, M., S. Fatemi, Y. Futaana, and H. Nilsson (2012), The interaction between the Moon and the solar wind, *Earth Planets Space*, *64*, 237–245.
Hutchinson, I. H. (2013), Near-lunar proton velocity distribution explained by electrostatic acceleration, *J. Geophys. Res. Space Physics*, *118*, 1825–1827, doi:10.1002/jgra.50277.
Kallio, E. (2005), Formation of the lunar wake in quasi-neutral hybrid model, *Geophys. Res. Lett.*, *32*, L06107, doi:10.1029/2004GL021989.
Khurana, K. K., C. T. Russell, and M. K. Dougherty (2007), Magnetic portraits of Tethys and Rhea, *Icarus*, *193*, 465–474, doi:10.1016/j.icarus.2007.08.005.
Kimura, S., and T. Nakagawa (2008), Electromagnetic full particle simulation of the electric field structure around the moon and the lunar wake, *Earth Planets Space*, *60*, 591–599.
Lue, C., Y. Futaana, S. Barabash, M. Wieser, M. Holmström, A. Bhardwaj, M. B. Dhanya, and P. Wurz (2011), Strong influence of lunar crustal fields on the solar wind flow, *Geophys. Res. Lett.*, *38*, L03202, doi:10.1029/2010GL046215.
Manfredi, G., S. Mola, and M. R. Feix (1993), Rescaling methods and plasma expansions into vacuum, *Phys. Fluids B*, *5*, 388–401.
McFadden, J. P., C. W. Carlson, D. Larson, M. Ludlam, R. Abiad, B. Elliott, P. Turin, M. Marckwordt, and V. Angelopoulos (2008), The THEMIS ESA plasma instrument and in-flight calibration, *Space Sci. Rev.*, *141*, 277–302.
Nakagawa, T. (2013), Ion entry into the wake behind a nonmagnetized obstacle in the solar wind: Two-dimensional particle-in-cell simulations, *J. Geophys. Res. Space Physics*, *118*, 1849–1860, doi:10.1002/jgra.50129.
Nakagawa, T., and S. Kimura (2011), Role of the solar wind magnetic field in the interaction of a non-magnetized body with the solar wind: An electromagnetic 2-D particle-in-cell simulation, *Earth Planets Space*, *67*, 477–486.
Ness, N. F. (1972), Interaction of the solar wind with the Moon, in *Solar Terrestrial Physics/1970*, Part II, edited by E. R. Dyer, pp. 159–205, D. Reidel Publ. Comp, Dordrecht.
Nishino, M. N., et al. (2009a), Pairwise energy gain-loss feature of solar wind protons in the near-Moon wake, *Geophys. Res. Lett.*, *36*, L12108, doi:10.1029/2009GL039049.
Nishino, M. N., et al. (2009b), Solar-wind proton access deep into the near-Moon wake, *Geophys. Res. Lett.*, *36*, L16103, doi:10.1029/2009GL039444.
Nishino, M. N., et al. (2010), Effect of the solar wind proton entry into the deepest lunar wake, *Geophys. Res. Lett.*, *37*, L12106, doi:10.1029/2010GL043948.
Ogilvie, K. W., J. T. Steinberg, R. J. Fitzenreiter, C. J. Owen, A. J. Lazarus, W. M. Farrell, and R. B. Torbert (1996), Observations of the lunar plasma wake from the WIND spacecraft on December 27, 1994, *Geophys. Res. Lett.*, *10*, 1255–1258, doi:10.1029/96GL01069.
Poppe, A. R., S. Fatemi, J. S. Halekas, M. Holmstrom, and G. T. Delory (2014), ARTEMIS observations of extreme diamagnetic fields in the lunar wake, *Geophys. Res. Lett.*, doi:10.1002/2014GL060280.
Roussos, E., J. Muller, S. Simon, A. Boesswetter, U. Motschmann, N. Krupp, M. Franz, J. Woch, K. K. Khurana, and M. Dougherty (2007), Plasma and fields in the wake of Rhea: 3d hybrid simulation and comparison with Cassini data, *Ann. Geophys.*, *26*, 619–637.
Sack, C., and H. Schamel (1987), Plasma expansion into vacuum – A hydrodynamic approach, *Phys. Rep.*, *156*, 311–395.
Saito, Y., et al. (2008), Solar wind proton reflection at the lunar surface: Low energy ion measurements by MAP-PACE onboard SELENE (KAGUYA), *Geophys. Res. Lett.*, *35*, L24205, doi:10.1029/2008GL036077.
Saito, Y., et al. (2010), Inflight performance and initial results of Plasma energy Angle and Composition Experiment (PACE) on SELENE (Kaguya), *Space Sci. Rev.*, *154*, 265.
Samir, U., K. H. Wright Jr., and N. H. Stone (1983), The expansion of a plasma into a vacuum: Basic phenomena and processes and applications to space plasma physics, *Rev. Geophys.*, *21*, 1631–1646, doi:10.1029/RG021i007p01631.
Schubert, G., and B. R. Lichtenstein (1974), Observations of Moon-plasma interactions by orbital and surface experiments, *Rev. Geophys.*, *12*, 592–626, doi:10.1029/RG012i004p00592.
Simon, S., J. Saur, F. M. Neubauer, U. Motschmann, and M. K. Dougherty (2009), Plasma wake of Tethys: Hybrid simulations versus Cassini MAG data, *Geophys. Res. Lett.*, *36*, L04108, doi:10.1029/2008GL036943.
Singh, N., and R. W. Schunk (1982), Numerical calculations relevant to the initial expansion of the polar wind, *J. Geophys. Res.*, *87*, 9154–9170, doi:10.1029/JA087iA11p09154.
Trávnicek, P., P. Hellinger, D. Schriver, and S. D. Bale (2005), Structure of the lunar wake: Two-dimensional global hybrid simulations, *Geophys. Res. Lett.*, *32*, L06102, doi:10.1029/2004GL022243.
Umeda, T., T. Kimura, K. Togano, K. Fukazawa, Y. Matsumoto, T. Miyoshi, N. Terada, T. K. M. Nakamura, and T. Ogino (2011), Vlasov simulation of the interaction between the solar wind and a dielectric body, *Phys. Plasmas*, *18*, 012908.
Wang, Y.-C., J. Muller, W.-H. Ip, and U. Motschmann (2011), A 3D hybrid simulation study of the electromagnetic field distributions in the lunar wake, *Icarus*, *216*, 415–425.

Wiehle, S., et al. (2011), First lunar wake passage of ARTEMIS: Discrimination of wake effects and solar wind fluctuations by 3D hybrid simulations, *Planet. Space Sci.*, *59*, 661–671.

Zhang, H., et al. (2012), Outward expansion of the lunar wake: ARTEMIS observations, *Geophys. Res. Lett.*, *39*, L18104, doi:10.1029/2012GL052839.

Zhang, H., K. K. Khurana, M. G. Kivelson, V. Angelopoulos, W. X. Wan, L. B. Liu, Q.-G. Zong, Z. Y. Pu, Q. Q. Shi, and W. L. Liu (2014), Three-dimensional lunar wake reconstructed from ARTEMIS data, *J. Geophys. Res. Space Physics*, doi:10.1002/2014JA020111.